2010 IEEE International Conference on Robotics and Automation
Anchorage Convention District
May 3-8, 2010, Anchorage, Alaska, USA

Homography-based Visual Servoing of an Aircraft for Automatic Approach and Landing

Tiago Gonçalves, José Azinheira and Patrick Rives

Abstract— **This paper proposes the Euclidean homography matrix as visual feature in an image-based visual servoing scheme in order to control an aircraft along the approach and landing phase. With a trajectory defined in the image space by a sequence of equidistant key images along the glidepath, an interpolation in the homography space is also proposed in order to reduce the database size and ensure the required smoothness of the control task. In addition, a pan-tilt control was taken into account to respect the dynamics of the aircraft during manoeuvres and in the presence of wind perturbations. An optimal control design based on the linearized model of the aircraft dynamics is then consider to cancel the visual error function. To demonstrate the proposed concept, simulation results under realistic atmospheric disturbances are presented.**

I. Introduction

Visual servoing refers to the use of visual data in order to control the motion of a robot [10] [12]. Depending on the nature of the visual data, or visual features, visual servoing schemes can be classified in two major groups: the position-based, or 3D, visual servoing (PBVS) and the image-based, or 2D, visual servoing (IBVS). While the PBVS uses the reconstructed pose from the visual data in order to control the robot, like no matter other pose sensor, the IBVS uses the visual data directly into the control loop. In IBVS, the error is then defined in terms of visual features and the controller to act in order to drive the visual features to a goal configuration that implicitly solves the problem of pose correction [6] [7]. For most of the visual servoing schemes proposed in the literature, the robot dynamics are, or can be assume as, ideal leading to kinematic control laws. The control of an aircraft, where the dynamics are not negligible, take us to a new kind of problems [8].

The intention of using vision systems for automatic landing or simply estimate the aircraft pose is not new. Flight tests of a vision-based autonomous landing relying on feature points on the runway were already referred by [9] whilst [5] present a feasibility study on pose determination for an aircraft night landing aid based on a model of the *Approach Lighting System* (ALS). Many other have followed in using visual servoing schemes for fixed/rotary-wings aircraft, and even airships, for different goals: autonomous aerial refueling [13] [15], stabilization with respect to a target [11] [1], linear structure following [22] [18] [14] and, naturally, automatic approach and landing [20] [17], [19] [16] [3] [4]. Most of the proposed schemes are PBVS, where the camera is used as a pose sensor along with a GPS, inertial sensors or even air data [9] in a filtering method. For IBVS schemes, the interaction matrix is crucial [6], allowing to relate the visual features with the state of the aircraft. Here, different types of visual features were considered: geometric model of the target [11] [13], binormalized Plücker coordinates of parallel lines [14], polar coordinates of the three parallel lines of the runway (both sides and central lines) [17] [3] [4] and the two side lines of the runway along with the horizon line and vanishing point [18]. Due to the standard geometry of the runway and decoupling capabilities, the last two schemes have been preferred in problems of automatic approach and landing.

In computer vision, a planar scene like the region around the runway plays an important role since it simplifies the computation of the projective transformation between two images of the same scene: the planar homography. The Euclidean homography, computed from the projective homography with the knowledge of an estimative of the calibration matrix, is then here considered as the visual feature in an image-based visual servoing scheme. In order to compute the projective homography matrix, a dense visual tracking was used [2][21], known by its accuracy since all the information in the image is used without intermediate processes of features extraction and matching and real-time performance.

This paper is organized as follows: In Section II some useful notations in visual servoing are introduced, along with the considered frames and the aircraft dynamics. In the same section, the two-views geometry is presented as the basis for the deduction of the interaction matrix as well as the path interpolation in Section III. The control aspects are then presented in Section IV, where the control law and the pan-tilt control are discussed in detail. The simulation results are finally shown and discussed in Section V while the final conclusions are given in Section VI.

This work is funded by the FP6 3rd Call European Commission Research Program under grant N.30839 - Project PEGASE

T. Gonçalves is with IDMEC/IST/TULisbon, 1 Av. Rovisco Pais, 1049-001 Lisbon, Portugal and with INRIA Sophia-Antipolis - Project ARobAS, 2004 Route des Lucioles, BP 93, 06902 Sophia-Antipolis Cedex, France t.goncalves@dem.ist.utl.pt, Tiago.Goncalves@sophia.inria.fr

J. Azinheira is with IDMEC/IST/TULisbon, 1 Av. Rovisco Pais, 1049-001 Lisbon, Portugal jraz@dem.ist.utl.pt

P. Rives is with INRIA Sophia-Antipolis - Project ARobAS, 2004 Route des Lucioles, BP 93, 06902 Sophia-Antipolis Cedex, France Patrick.Rives@inria.sophia.fr

II. Theoretical Background

A. Frames and Notations

The rigid-body motion of a frame $\mathcal{F}_b$ with respect to a frame $\mathcal{F}_a$ by a rotation ${}^a\mathbf{R}_b \in \mathbb{SO}(3)$ and a translation ${}^a\mathbf{t}_b \in \mathbb{R}^3$, is usually expressed in homogeneous coordinates as

$$ {}^a\mathbf{T}_b = \begin{bmatrix} {}^a\mathbf{R}_b & {}^a\mathbf{t}_b \\ \mathbf{0} & 1 \end{bmatrix} \in \mathbb{SE}(3) \tag{1} $$

where $\mathbf{0}$ denotes a matrix of zeros with the appropriate dimensions. The corresponding velocity screw ${}^a\mathbf{V}_{ab} = \left[\mathbf{v}^\top, \omega^\top\right]^\top \in \mathbb{R}^6$, which definition if given by

$$ {}^a\widehat{\mathbf{V}}_{ab} = {}^a\dot{\mathbf{T}}_b {}^a\mathbf{T}_b^{-1} = \begin{bmatrix} \widehat{\omega} & \mathbf{v} \\ \mathbf{0} & 0 \end{bmatrix} \in \mathfrak{se}(3), \tag{2} $$

denotes the velocity of the frame $\mathcal{F}_b$ with respect to the frame $\mathcal{F}_a$ and viewed from $\mathcal{F}_a$. The angular velocity tensor $\widehat{\omega} \in \mathfrak{so}(3)$ is the skew-symmetric matrix corresponding to the angular velocity vector ω such that $\omega \times \mathbf{X} = \widehat{\omega}\mathbf{X}$, where $\mathbf{X} \in \mathbb{R}^3$ is a generic vector. The inverse operation will be denoted by $\text{vec}(\widehat{\omega}) = \omega$. Also important in the present paper is the definition of stacked matrix, denoted by the superscript "^{s}", where each column is stacked into a single column vector.

B. Aircraft Dynamic Model

Let $\mathcal{F}_0$ be the inertial frame, also called NED for North-East-Down, whose origin coincides with the desirable touchdown point in the runway. The latter, unless explicitly indicated and without loss of generality, will be considered aligned with North. The aircraft linear velocity $\mathbf{v} = [u, v, w]^\top \in \mathbb{R}^3$, as well as its angular velocity $\omega = [p, q, r]^\top \in \mathbb{R}^3$, are expressed in the aircraft body frame $\mathcal{F}_b$ whose origin is at the center of gravity and where u is defined towards the aircraft nose, v towards the right wing and w downwards, as illustrated in Fig. 1. The attitude, or orientation, of the aircraft with respect to the inertial frame $\mathcal{F}_0$ is stated in terms of Euler angles $\Phi = [\phi, \theta, \psi]^\top \subset \mathbb{R}^3$, the roll, pitch and yaw angles respectively. Since both linear and angular velocities of the aircraft are expressed in the body frame $\mathcal{F}_b$, the Coriolis theorem must be invoked and kinematic equations appear naturally relating the angular velocity with the time derivative of the Euler angles $\dot{\Phi} = \mathbf{R}^{-1}\omega$ and the instantaneous linear velocity with the time derivative of the NED position $[\dot{N}, \dot{E}, \dot{D}]^\top = \mathbf{S}^\top\mathbf{v}$, where $\mathbf{S}$ denotes de *Direction Cosine Matrix* (DCM).

For control purposes, the nonlinear dynamic model of the aircraft along with the kinematic relations are linearized around a given equilibrium flight condition, a function of the true airspeed $\mathbf{V}_{T_0}$ and the altitude h_0. This equilibrium or trim flight is frequently chosen to be a steady wing-level flight, without presence of wind disturbances, also justified here since non-straight landing approaches are not considered in the present paper. The resultant linear model is then a function of the perturbations in the state $\mathbf{x}$ and input $\mathbf{u}$

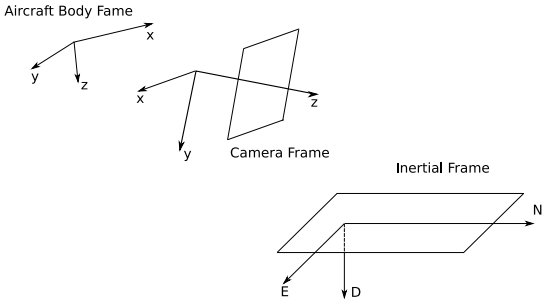

Fig. 1. Illustration of the considered frames and notations.

vectors as

$$ \begin{bmatrix} \dot{\mathbf{x}}_v \\ \dot{\mathbf{x}}_h \end{bmatrix} = \begin{bmatrix} \mathbf{A}_v & \mathbf{0} \\ \mathbf{0} & \mathbf{A}_h \end{bmatrix} \begin{bmatrix} \mathbf{x}_v \\ \mathbf{x}_h \end{bmatrix} + \begin{bmatrix} \mathbf{B}_v & \mathbf{0} \\ \mathbf{0} & \mathbf{B}_h \end{bmatrix} \begin{bmatrix} \mathbf{u}_v \\ \mathbf{u}_h \end{bmatrix} \tag{3} $$

describing the dynamics of the two resultant decoupled longitudinal and lateral motions. The longitudinal, or vertical, state vector is $\mathbf{x}_v = [u, w, q, \theta]^\top \in \mathbb{R}^4$ and the respective input vector $\mathbf{u}_v = [\delta_E, \delta_T]^\top \in \mathbb{R}^2$ (elevator and throttle) while in the lateral, or horizontal, case the state vector is $\mathbf{x}_h = [v, p, r, \phi]^\top \in \mathbb{R}^4$ and the respective input vector $\mathbf{u}_h = [\delta_A, \delta_R]^\top \in \mathbb{R}^2$ (aileron and rudder). Since the equilibrium flight condition is slowly varying for manoeuvres as the final segment of the landing phase, the linearized model in (3) can be then considered as constant all along the glidepath.

C. Two-Views Geometry

The onboard camera frame $\mathcal{F}_c$, mounted on a pan-tilt system rigidly attached to the aircraft, has its origin at the center of projection of the camera, also called pinhole. The corresponding z-axis, perpendicular to the image plane, lies on the optical axis while the x- and y- axis are defined towards right and down, respectively. Note that the camera frame $\mathcal{F}_c$ is not in agreement with the one usually defined in flight mechanics.

Let $\mathcal{P}$ be a 3D point whose coordinates in the current camera frame ${}^c\mathbf{X}$ could be related with those ${}^*\mathbf{X}$ in a second camera frame $\mathcal{F}_*$, denoted reference camera frame, by

$$ {}^c\mathbf{X} = {}^c\mathbf{R}_* {}^*\mathbf{X} + {}^c\mathbf{t}_* \tag{4} $$

Considering that $\mathcal{P}$ lies on a plane Π defined by the unit normal vector ${}^*\mathbf{n} \in \mathbb{R}^3$ and the distance d^* such as

$$ \frac{1}{d^*} {}^*\mathbf{n}^\top {}^*\mathbf{X} = 1 \tag{5} $$

there exists a linear transformation ${}^c\mathbf{H}_*$ between both coordinates given by

$$ {}^c\mathbf{H}_* = {}^c\mathbf{R}_* + \frac{1}{d^*} {}^c\mathbf{t}_* {}^c\mathbf{n}_*^\top \tag{6} $$

where ${}^c\mathbf{H}_* \in \mathbb{R}^{3\times3}$ is the so-called Euclidean homography matrix. Therefore, given a set of matched point, lines or even dense information from two images $\mathcal{I}$ and $\mathcal{I}^*$, it is possible to compute the projective homography matrix $\mathbf{G} \in \mathbb{R}^{3\times3}$ up

to a scale factor. Knowing an estimative of the calibration matrix $\mathbf{K}$, the Euclidean homography matrix $\mathbf{H}$ can then be computed also up to a scale factor

$$\mathbf{H} = \mathbf{K}^{-1}\mathbf{G}\mathbf{K} \tag{7}$$

The calibration matrix, or the camera intrinsical parameters, $\mathbf{K} \in \mathbb{R}^{3\times3}$ is defined as follows

$$\mathbf{K} = \begin{bmatrix} f_x & fs & p_{x_0} \\ 0 & f_y & p_{y_0} \\ 0 & 0 & 1 \end{bmatrix} \tag{8}$$

where, the coordinates $\mathbf{p}_0 = [p_{x_0}, p_{y_0}, 1]^\top \in \mathbb{R}^3$ define the principal point, corresponding to the intersection between the image plane and the optical axis, s is the skew factor (zero for most of the cameras) and finally, f_x and f_y are the focal lengths in both directions such that when $f_x = f_y$ the camera sensor presents square pixels.

III. Homography-based Visual Servoing

In image-based, or 2D, visual servoing (IBVS) the control law is expressed directly in the image space. In contrast with other approaches, the IBVS does not need to reconstruct explicitly the pose with respect to the inertial frame. Instead, the visual signal $\mathbf{s}$ is used directly into the control law such that reaching a certain reference configuration $\mathbf{s}^*$ the robot presents the intended pose. In the present paper, the visual signal considered is then the stacked version of the Euclidean homography matrix $\mathbf{H}^s$.

A. Interaction Matrix

The interaction matrix $\mathbf{L_s} \in \mathbb{R}^{k\times6}$ plays a crucial role for IBVS schemes. It relates variations of the visual signal vector $\mathbf{s} \in \mathbb{R}^k$ with the instantaneous velocity of the camera ${}^c\mathbf{V}$ as

$$\dot{\mathbf{s}} = \mathbf{L_s}\,{}^c\mathbf{V} \tag{9}$$

Let us now consider the proposed visual signal $\mathbf{s}$ as ${}^c\mathbf{H}_*$, the Euclidean homography matrix, denoted in the following as $\mathbf{H}$ for simplicity reasons. Admitting the vector ${}^*\mathbf{n}/d^*$ as slowly varying, the time derivative of $\mathbf{H}$ is thus given by

$$\dot{\mathbf{H}} = \dot{\mathbf{R}} + \frac{1}{d^*}\dot{\mathbf{t}}\,{}^*\mathbf{n}^\top \tag{10}$$

Now, it is known that both $\dot{\mathbf{R}}$ and $\dot{\mathbf{t}}$ are related to the velocity screw ${}^c\mathbf{V}_{c*} = [\mathbf{v}^\top, \omega^\top]^\top$ which could be determined using the definition in (2)

$${}^c\widehat{\mathbf{V}}_{c*} = \begin{bmatrix} \dot{\mathbf{R}}\mathbf{R}^\top & \dot{\mathbf{t}} - \dot{\mathbf{R}}\mathbf{R}^\top\mathbf{t} \\ \mathbf{0} & 0 \end{bmatrix} = \begin{bmatrix} \widehat{\omega} & \mathbf{v} \\ \mathbf{0} & 0 \end{bmatrix} \tag{11}$$

from where, $\dot{\mathbf{R}} = \widehat{\omega}\mathbf{R}$ and $\dot{\mathbf{t}} = \mathbf{v} + \widehat{\omega}\mathbf{t}$. Using such result back in (10) results on

$$\dot{\mathbf{H}} = \widehat{\omega}\mathbf{H} + \frac{1}{d^*}\mathbf{v}\,{}^*\mathbf{n}^\top \tag{12}$$

Finally, in order to obtain the visual signal vector $\mathbf{s}$, the stacked version of the homography matrix $\dot{\mathbf{H}}^s$ must be considered and, as a result, the interaction matrix is given by

$$\mathbf{L_s} = \begin{bmatrix} \mathbf{I}^* n_1/d^* & -\widehat{\mathbf{H}}_1 \\ \mathbf{I}^* n_2/d^* & -\widehat{\mathbf{H}}_2 \\ \mathbf{I}^* n_3/d^* & -\widehat{\mathbf{H}}_3 \end{bmatrix} \in \mathbb{R}^{9\times6} \tag{13}$$

where, $\mathbf{I}$ denotes the 3×3 identity matrix and $\mathbf{H}_i$ is the ith column of the matrix as well as n_i is the ith element of the vector. Note that, $\widehat{\omega}\mathbf{H}$ is the external product of ω with all the columns of $\mathbf{H}$ and then $\omega\times\mathbf{H}_i = -\mathbf{H}_i\times\omega = -\widehat{\mathbf{H}}_i\omega$.

The velocity screw defined in (11) and considered till here denotes the velocity of the reference frame $\mathcal{F}_*$ with respect to the airborne camera frame $\mathcal{F}_c$ and viewed from $\mathcal{F}_c$, *i.e.* ${}^c\mathbf{V}_{c*}$, which is not in agreement with the aircraft velocity screw that must be applied to a general control law. Instead, it shall be expressed with respect to $\mathcal{F}_*$ and viewed from the aircraft body frame $\mathcal{F}_b$, *i.e.* ${}^b\mathbf{V}_{*c}$. In this manner, knowing the following relation from the adjoint map

$${}^c\widehat{\mathbf{V}}_{c*} = {}^c\mathbf{T}_b\,{}^b\widehat{\mathbf{V}}_{c*}\,{}^c\mathbf{T}_b^{-1} = {}^b\mathbf{T}_c^{-1}(-{}^b\widehat{\mathbf{V}}_{*c})\,{}^b\mathbf{T}_c, \tag{14}$$

it is possible to find the velocity screw transformation ${}^c\mathbf{W}_b$ given by

$${}^c\mathbf{W}_b = \begin{bmatrix} {}^b\mathbf{R}_c^\top & -{}^b\mathbf{R}_c^\top\,{}^b\widehat{\mathbf{t}}_c \\ \mathbf{0} & {}^b\mathbf{R}_c^\top \end{bmatrix} \tag{15}$$

such that

$${}^c\mathbf{V}_{c*} = -{}^c\mathbf{W}_b\,{}^b\mathbf{V}_{*c} \tag{16}$$

where ${}^b\mathbf{R}_c$ and ${}^b\mathbf{t}_c$ define the pose of the onboard camera frame $\mathcal{F}_c$ with respect to the aircraft body frame $\mathcal{F}_b$. Finally, using (13) into (9) along with (15) results as follows

$$\dot{\mathbf{s}} = {}^c\dot{\mathbf{H}}_*^s = -\mathbf{L_s}\,{}^c\mathbf{W}_b\,{}^b\mathbf{V}_{*c} \tag{17}$$

B. Error function

The objective of an IBVS scheme is to reach a certain configuration expressed in terms of the considered features $\mathbf{s} = \mathbf{s}^*$, here the Euclidean homography matrix ${}^c\mathbf{H}_*^s$. Because the considered dense visual tracking is achieved by directly estimate the projective transformation between the image taken from the airborne camera and a given reference image, the reference images are then the key to relate the motion of the aircraft $\mathcal{F}_b$ with respect to the inertial frame $\mathcal{F}_0$ through the airborne camera $\mathcal{F}_c$. Therefore, the trajectory to follow shall be defined by images.

Since the approach glidepath is a well-defined trajectory the existence of a database composed by images $\{\mathcal{I}_k^*\}_{k=0}^N$, taken all along the reference path for equidistant longitudinal distances $d_\mathcal{I}$, can be considered, as illustrated in Fig. 2. The easiest way to define the error function $\mathbf{s}-\mathbf{s}^*$ to be minimized by the control law is then to establish

$$\mathbf{s}^* = \mathbf{H}^{*s} = \mathbf{I}^s \tag{18}$$

such that the current and the reference image match for $\mathbf{s} - \mathbf{s}^* = 0$. Due to the slow longitudinal dynamics of the aircraft, an acceptable result can be achieved using a

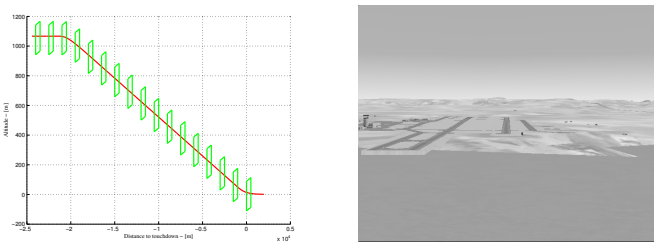

Fig. 2. Illustration of the sequence of reference images along the path to follow along with one of the images from the database.

sufficiently small distance $d_{\mathcal{I}}$ between consecutive reference images but the size of the needed database will be significant. For larger $d_{\mathcal{I}}$ and consequent altitude error, an important oscillation on the longitudinal motion of the aircraft is verified. An interpolation of the visual reference $\mathbf{s}^*$ is then desirable.

C. Path Interpolation

Let us consider $\left\{{}^{k-1}\mathbf{H}_k\right\}_{k=1}^{N}$, the set of Euclidean homographies, computed off-line, between two consecutive reference images $\mathcal{I}_k^*$. Since the glidepath is essentially a straight line, it is possible to consider an interpolation in the homography space as

$$\mathbf{H}_k^*(\mu) = \mathbf{I} + \mu\left({}^{k-1}\mathbf{H}_k - \mathbf{I}\right) \tag{19}$$

such that it corresponds to an interpolation in the Euclidean space since ${}^{k-1}\mathbf{R}_k = \mathbf{I}$ and, as a consequence,

$$\begin{aligned}\mathbf{H}_k^*(\mu) &= \mathbf{I} + \mu\left(\mathbf{I} + \tfrac{1}{d_k^*}{}^{k-1}\mathbf{t}_k{}^*\mathbf{n}_k^\top - \mathbf{I}\right)\\ &= \mathbf{I} + \tfrac{\mu}{d_k^*}{}^{k-1}\mathbf{t}_k{}^*\mathbf{n}_k^\top\end{aligned} \tag{20}$$

where $\mu \in [0,1]$ is the interpolator parameter.

The interpolator parameter μ, associated to the longitudinal distance between the current camera frame $\mathcal{F}_c$ and the reference camera frame $\mathcal{F}_*$, can be computed directly from the estimated Euclidean homography ${}^c\mathbf{H}_*$ as follows

$$\mu = \frac{d_k^*}{d_{\mathcal{I}}}\left[1,0,0\right]\mathrm{vec}\left({}^c\mathbf{H}_* - {}^c\mathbf{H}_*^\top\right) \tag{21}$$

which, for small attitude errors and knowing that ${}^*\mathbf{n} \approx [0,1,0]^\top$ then

$$\mu \approx \frac{{}^c t_{*_z}}{d_{\mathcal{I}}} \tag{22}$$

IV. Control Design

The standard LQR optimal control technique was chosen for the controller design, based on the linearized model in (3) for both longitudinal and lateral motions. Since not all the states are expected to be driven to zero but to a given reference, the feedback is more conveniently expressed as an optimal output error feedback defined as

$$\mathbf{u} = -\mathbf{k}\left(\mathbf{x} - \mathbf{x}^*\right) \tag{23}$$

where, $\mathbf{u}$ is the control action and $\mathbf{k}$ the optimal state feedback gain. In order to compensate static errors by wind disturbances and, namely from velocity, altitude and lateral errors, additional integrative states were considered.

The objective of the present homography-based visual servoing scheme is to express the control law into the form of (23) but as a function of the visual information, here related with the pose of the aircraft by means of the Euclidean homography matrix. As a consequence, the pose state vector $\mathbf{P} = [N, E, D, \phi, \theta, \psi]^\top \in \mathbb{R}^6$ is given differently from the velocity screw $\mathbf{V} = [u, v, w, p, q, r]^\top \in \mathbb{R}^6$, which could be provided from an existent *Inertial Navigation System* (INS) or from some filtering method based on the estimated pose. Thus, the control law (23) is more correctly expressed as

$$\mathbf{u} = -\mathbf{k}_{\mathbf{P}}\left(\mathbf{P} - \mathbf{P}^*\right) - \mathbf{k}_{\mathbf{V}}\left(\mathbf{V} - \mathbf{V}^*\right) \tag{24}$$

where, $\mathbf{k}_{\mathbf{P}}$ and $\mathbf{k}_{\mathbf{V}}$ are the controller gains relative to the pose and velocity states, respectively.

A. Control Law

Since not all the variables in the interaction matrix are usually known, it is common in visual servoing to approximate the interaction matrix as constant and equal to the one at the desired configuration $\mathbf{L}_{\mathbf{s}} = \mathbf{L}_{\mathbf{s}}^*$. In addition, for small displacements, the relation (17) can be integrated around the same configuration resulting in

$$\mathbf{s} - \mathbf{s}^* = \mathbf{H}^s - \mathbf{H}^{*s} = -\mathbf{L}_{\mathbf{s}}^{*c}\mathbf{W}_b{}^b\mathbf{W}_0\left(\mathbf{P} - \mathbf{P}^*\right) \tag{25}$$

where ${}^b\mathbf{V} = {}^b\mathbf{W}_0\dot{\mathbf{P}}$ correspond to the kinematic relations already referred, *i.e.* ${}^b\mathbf{W}_0 = diag([\mathbf{S}_0, \mathbf{R}_0])$. Using the same trim point as for the aircraft linear model, the desired interaction matrix results in

$$\mathbf{L}_{\mathbf{H}}^* = -\left.\mathbf{L}_{\mathbf{s}}{}^c\mathbf{W}_0\right|_* = [\mathbf{J}_{\mathbf{v}}, \mathbf{J}_{\omega}] \tag{26}$$

such that

$$\mathbf{J}_{\mathbf{v}} = \frac{1}{h_t}\begin{bmatrix}\mathbf{0} & -c_{\theta_I}\mathbf{I} & s_{\theta_I}\mathbf{I}\end{bmatrix}^\top \tag{27}$$

and

$$\mathbf{J}_{\omega} = \begin{bmatrix} 0 & 0 & 0 & 0 & 0 & -1 & 0 & 1 & 0 \\ 0 & 0 & 1 & 0 & 0 & 0 & -1 & 0 & 0 \\ 0 & -c_{\theta_t} & 0 & c_{\theta_t} & 0 & s_{\theta_t} & 0 & -s_{\theta_t} & 0 \end{bmatrix}^\top \tag{28}$$

where, $c_\theta = \cos\theta$, $s_\theta = \sin\theta$. The pitch angle $\theta_t = \theta_0 + \gamma$ corresponds to the trim pitch θ_0 modified for the descent condition $\gamma \approx -3^\circ$ and $\theta_I = \theta_t + \theta_c \approx \gamma$ to the pitch angle of the onboard camera ($\theta_c \approx \theta_0$) wrt the horizontal plane. The distance $h_t = h_k^* - z_c\cos(\theta_0 + \gamma) + x_c\sin(\theta_0 + \gamma)$ corresponds to the altitude above ground of the reference camera frame $\mathcal{F}_*$ placed at ${}^b\mathbf{t}_c = [x_c, 0, z_c]^\top$ wrt the aircraft body frame $\mathcal{F}_b$.

The proposed homography-based visual servoing control law is then finally given by

$$\mathbf{u} = -\mathbf{k}_{\mathbf{P}}\mathbf{L}_{\mathbf{H}}^{*+}\left({}^c\mathbf{H}_*^s - \mathbf{H}_k^{*s}(\mu)\right) - \mathbf{k}_{\mathbf{V}}\left(\mathbf{V} - \mathbf{V}^*\right) \tag{29}$$

where $\mathbf{L}^+$ denotes the pseudo-inverse of the interaction matrix.

B. Pan-Tilt Control

The pan-tilt system is a fundamental tool in order to respect the dynamics of the aircraft in IBVS schemes. Indeed, the pan-tilt control allows not only to keep the target in the field-of-view of the camera during manoeuvres, without influence on the dynamics of the aircraft, but also to ensure the conditions stated above even in the presence of external perturbations. Perturbations like the wind change the attitude trim condition of the flight imposing some difficulties to the visual tracking as well as some errors on the assumptions done for the control law, affecting the accuracy of the positioning of the aircraft.

With the objective of maintaining the camera pointing in the same reference direction $\Phi^* = [0, -\theta_0, 0]^\top$, the pan-tilt control can be performed by a simple control law as

$$\Phi_{pt}(k+1) = \Phi_{pt}(k) - \mathbf{k}_{pt}\Phi_e(k) \tag{30}$$

where, the initial pan-tilt angles are $\Phi_{pt}(0) = \Phi^*$, $\mathbf{k}_{pt}$ denotes the gains of the control law and $\Phi_e(k)$ the attitude error retrieved from the relation in (25), at the time increment k. Due to the new orientation of the onboard camera, this same attitude error Φ_e must be corrected as follows

$$\mathbf{R}(\Phi_e) = \mathbf{R}(\Phi_e)\mathbf{R}(\Phi^* - \Phi_{pt}) \tag{31}$$

in order to compensate the pan-tilt orientation on the estimation of the aircraft pose error. Due to the negligible positioning of the onboard camera wrt the aircraft body frame over the precision of the estimation, no corrections on the estimated position error are considered.

V. Results

A. Simulation environment

The homography-based visual servoing here proposed has been developed and tested in a simulation framework where the realistic non-linear aircraft model provided by Alenia Aeronautica company is implemented in Matlab/Simulink along with the control aspects, the image processing algorithms in C/C++ and the simulated image generated by the FlightGear flight simulator. The non-linear aircraft model corresponds to a generic category B business jet with $50m/s$ of stall speed and $20m$ of wing span. This simulation framework has also the capability to simulate atmospheric perturbations like steady wind as well as different levels of turbulence.

B. Experimental conditions

The chosen airport scenario was the Marseilles-Marignane Airport with a nominal initial position defined by an altitude of $450m$ and a longitudinal distance to the runway of $9500m$, resulting in a 3° descent for an airspeed of $60m/s$. In order to present an illustrative set of results and to verify the robustness of the proposed visual servoing scheme, it was imposed an initial lateral error of $50m/s$, an altitude error of $30m$ and a steady wind composed by $10m/s$ headwind and $1m/s$ of crosswind. The airborne camera initial pose is ${}^b\mathbf{P}_c^* = [4m, 0m, 0.1m, 0, -8^\circ, 0]^\top$. What concerns the reference images of the database, three distinct distances were considered $\{250m, 500m, 1000m\}$ in order to evaluate the performance of the proposed scheme along with the interpolation method till the limit of robustness of the visual tracking. From the $100m$ of altitude till the touchdown, this distance is reduced to the value of $50m$ due to limitations of the visual tracking. Indeed, the high pixels displacement on the image verified for low altitudes is not compatible to an iterative algorithm like a dense visual tracker. The simulation framework operates with a $50ms$, or $20Hz$, sampling rate.

C. Results

For the following figures, the results of the three different distance between the images of the database are presented simultaneously and identified in agreement with the legend in Fig. 3(b). When available, the corresponding references are presented by a black line.

Let us start with the pitch θ and yaw ψ attitude angles of the aircraft presented in Fig. 3(c) and Fig. 3(f). The results obtained for the three conditions are very similar. Indeed, this fact is not surprising taken into account that the attitude estimation errors provided by the visual tracker are often below 1° for transient responses and below 0.1° in steady state, one of the reasons why they were used for the pan-tilt control in Fig. 3(g) and Fig. 3(h). In addition, the attitude of the aircraft is not contemplated by the interpolation method, remaining constant all along the glidepath, not depended then from the considered distances. However, it is possible to identify more significant oscillations associated to the distance of $1000m$, with a maximum discrepancy of 0.5° for both attitude angles, induced by the errors related to the altitude and lateral error states.

In what concerns the positioning of the aircraft, notably the altitude and lateral error, presented in Fig. 3(b) and in Fig. 3(e), it is notable here the influence of the distance between reference images on the behavior of the aircraft. In more detail, it is even possible to identify the changes of reference images on the altitude error in Fig. 3(b) for the distance of $1000m$ which contrast with the smoothness of the altitude error correction for a distance of $250m$. However, even the worst case stills acceptable since the true airspeed oscillation is bounded for approximately $0.5m/s$ and the lateral error between $-4m$ and $6m$, not far from the other solutions. The cause of such differences is then the effort realized by the visual tracker in order to correspond the current image with the reference image $1000m$ away. To conclude, it should be mentioned the global convergence for about $2000m$ before the touchdown, corresponding to $100m$ of altitude, where the distance between images of the database is reduced to $50m$.

VI. Conclusions

In the present paper, an homography-based visual servoing scheme for an automatic approach and landing of an aircraft was proposed. The trajectory defined in the image space and

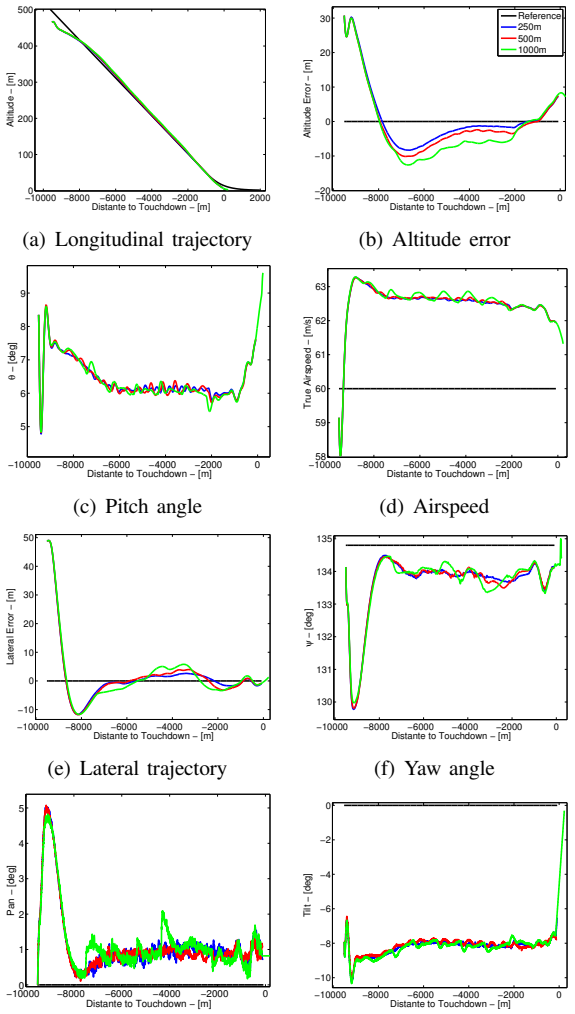

(a) Longitudinal trajectory (b) Altitude error

(c) Pitch angle (d) Airspeed

(e) Lateral trajectory (f) Yaw angle

(g) Pan angle (h) Tilt angle

Fig. 3. Results from the homography-based control schemes for the three distances in the presence of wind.

composed by a sequence of images show clearly to be able to correct the initial pose error and to land the aircraft even in the presence of windy conditions. In order to improve the basis scheme, an interpolation on the homography space(for the particular case of the translation) was proposed to avoid oscillation induced by a discrete visual reference like an image is. In addition, a pan-tilt control was also implemented to respect the aircraft dynamics during manoeuvres and to deal with the presence of wind, a common problem in visual servoing schemes applied to the aircraft navigation. Despite the inherent sensibility of vision tracking algorithm to the non-planarity of the scene and the high pixels displacement for low altitudes, a shorter distance between the images of the database was enough to deal with potential problems. The inexistence of a filtering method prove the robustness of the proposed scheme under real estimation errors and the reliability of the used dense visual tracking. These results clearly justifies further studies to complete the validation, finding a more reliable solution for the last meters of altitude, and the eventual implementation of this system on a real aircraft.

REFERENCES

[1] J.R. Azinheira, P. Rives, J.R.H. Carvalho, G.F. Silveira, de Paiva, E.C., and S.S. Bueno. Visual servo control for the hovering of an outdoor robotic airship. In *IEEE International Conference on Robotics and Automation*, volume 3, pages 2787–2792, May 2002.

[2] S. Behimane and E. Malis. Real-time image-based tracking of planes using efficient second-order minimization. In *IEEE International Conference on Intelligent Robot and Systems*, volume 1, pages 943–948, September 2004.

[3] O. Bourquardez and F. Chaumette. Visual servoing of an airplane for alignment with respect to a runway. In *IEEE International Conference on Robotics and Automation*, pages 1330–1355, April 2007.

[4] O. Bourquardez and F. Chaumette. Visual servoing of an airplane for auto-landing. In *IEEE International Conference on Intelligent Robots and Systems*, pages 1314–1319, November 2007.

[5] G.B. Chatterji, K. Menon, P., and B. Sridhar. Vision-based position and attitude determination for aircraft night landing. *AIAA Journal of Guidance, Control and Dynamics*, 21(1), January 1998.

[6] F. Chaumette and S. Hutchinson. Visual servo control, part i: Basic approaches. *IEEE Robotics and Automation Magazine*, 13(4):82–90, December 2006.

[7] F. Chaumette and S. Hutchinson. Visual servo control, part ii: Advanced approaches. *IEEE Robotics and Automation Magazine*, 14(1):109–118, March 2007.

[8] P.I. Corke and M.C. Good. Dynamic effects in visual closed-loop systems. *IEEE Transactions on Robotics and Automation*, 12(5):671–683, 1996.

[9] E.D. Dickmanns and F.R. Schell. Autonomous landing of airplanes by dynamic machine vision. *IEEE Workshop on Application on Computer Vision*, pages 172–179, 1992.

[10] B. Espiau, F. Chaumette, and P. Rives. A new approach to visual servoing in robotics. *IEEE Transactions on Robotics and Automation*, 8(3):313–326, June 1992.

[11] T. Hamel and R. Mahony. Visual servoing of an under-actuated dynamics rigid-body system: an image-based approach. In *IEEE Transactions on Robotics and Automation*, volume 18, pages 187–198. April 2002.

[12] S. Hutchinson, G. Hager, and P. Corke. A tutorial on visual servo control. *IEEE Transactions on Robotics and Automation*, 12(5):651–670, 1996.

[13] J. Kimmett, J. Valasek, and J. L. Junkins. Vision based controller for autonomous aerial refueling. In *Conference on Control Applications*, pages 1138–1143, September 2002.

[14] R. Mahony and T. Hamel. Image-based visual servo control of aerial robotic systems using linear images features. In *IEEE Transaction on Robotics*, volume 21, pages 227–239. April 2005.

[15] R. Mati, L. Pollini, A. Lunghi, and M. Innocenti. Vision-based autonomous probe and drogue aerial refueling. In *Conference on Control and Automation*, pages 1–6, June 2006.

[16] A.A. Proctor and E.N. Johnson. Vision-only aircraft flight control methods and test results. In *AIAA Guidance, Navigation, and Control Conference and Exhibit*, August 2004.

[17] P. Rives and J.R. Azinheira. Visual auto-landing of an autonomous aircraft. Research Report 4606, INRIA Sophia-Antilopis, November 2002.

[18] P. Rives and J.R. Azinheira. Linear structure following by an airship using vanishing point and horizon line in visual servoing schemes. In *IEEE International Conference on Robotics and Automation*, volume 1, pages 255–260, 2004.

[19] S. Saripalli, J.F. Montgomery, and G.S. Sukhatme. Visually-guided landing of an unmanned aerial vehicle. In *IEEE Transaction on Robotics*, volume 19, pages 371–381. 2003.

[20] C.S. Sharp, O. Shakernia, and S.S. Sastry. A vision system for landing an unmanned aerial vehicle. In *IEEE International Conference on Robotics and Automation*, volume 2, pages 1720– 1727, May 2002.

[21] G. Silveira and E. Malis. Real-time visual tracking under arbitrary illumination changes. In *IEEE Conference on Computer Vision and Pattern Recognition*, pages 1–6, June 2007.

[22] G.F. Silveira, J.R. Azinheira, P. Rives, and S.S. Bueno. Line following visual servoing for aerial robots combined with complementary sensors. In *IEEE International Conference on Robotics and Automation*, pages 1160–1165, July 2003.